




Effect of high pressure on temperature dependences of the resistivity in the ab-plane of $Y_{0.77}Pr_{0.23}Ba_2Cu_3O_{7-\delta}$ single crystals

A. Chroneos^{1,2,*} , G. Ya. Khadzhai³, I. L. Goulatis³, A. V. Mazepulin³, M. V. Korobkov³, and R. V. Vovk³

¹Department of Electrical and Computer Engineering, University of Thessaly, 38221 Volos, Greece

²Department of Materials, Imperial College, London SW7 2AZ, UK

³V.N. Karazin, Svobody Sq, Kharkiv National University, Kharkiv 61022, Ukraine

Received: 8 January 2022

Accepted: 22 February 2022

Published online:

16 March 2022

© The Author(s) 2022

ABSTRACT

In the present work, we investigated the influence of high hydrostatic pressure up to 11 kbar on the conductivity in the basal ab-plane of medium-doped with praseodymium ($x \approx 0.23$) single-crystal $Y_{1-x}Pr_xBa_2Cu_3O_{7-\delta}$ samples. It was determined that, in contrast to the pure $YBa_2Cu_3O_{7-\delta}$ samples with the optimal oxygen content, the application of high pressure leads to the formation of phase separation in the basal plane of $Y_{0.77}Pr_{0.23}Ba_2Cu_3O_{7-\delta}$ single crystals. Possible mechanisms of the effect of Pr doping and high pressure on the two-step resistive transition to the superconducting state are discussed. It was determined that in the normal state, the conductivity is metallic and is limited by phonons scattering (Bloch-Grüneisen regime) and defects. The fluctuation conductivity is considered within the Lorentz-Doniach model. Hydrostatic pressure, accompanied by a decrease in anisotropy, leads to a decrease in the residual and phonon resistances. Debye temperature and coherence length are independent of pressure. The applicability of the McMillan formula in the presence of significant anisotropy is discussed.

1 Introduction

The use of high-pressure technologies to study the critical characteristics of high-temperature superconductor (HTSC) materials continues to be one of the most promising experimental techniques that allow not only checking the adequacy of theoretical models but also finding empirical ways to improve their

electrical transport characteristics and increase critical parameters [1, 2]. This is particularly important, given that, despite the 35-year history of intensive theoretical and experimental research (from the discovery of HTSC in 1986 [3]), it is not possible to overcome the threshold of 200 K of the critical temperature (T_c) [4, 5]. In essence, the microscopic mechanism of HTSC remains unclear until now [1, 6].

Address correspondence to E-mail: alexander.chroneos@imperial.ac.uk

There are a number of reasons to investigate HTSC cuprates, and in particular, the 1–2–3 system where Y is partially replaced with Pr [7, 8]. Firstly, the compounds of the 1–2–3 system have a sufficiently high T_c , making it possible to carry out measurements at temperatures exceeding the temperature of liquid nitrogen [9, 10]. Secondly, the partial replacement of Y with Pr, in contrast to replacement with other rare earth elements, allows smoothly varying the electrical resistance and critical characteristics of this compound by gradually suppressing their conducting parameters [11–14] (the so-called “praseodymium anomaly”). Thirdly, in the $Y_{1-x}Pr_xBa_2Cu_3O_{7-\delta}$ compounds with the optimal oxygen content [15, 16], the so-called nonequilibrium state does not arise, which in pure oxygen-deficient $YBa_2Cu_3O_{7-\delta}$ samples can be quite easily induced by a jump in temperature, aging [17, 18] or high-pressure applications [19, 20].

The latter point is important for pure samples, where it is often necessary to use specific techniques that allow one to distinguish between the so-called true pressure effect [21, 22] (caused by a change in the parameters of the crystal lattice of interlayer interaction, electron–phonon interaction, etc.) and the relaxation effect [23, 24] (due to the redistribution of the labile component). Only a few previous studies were devoted to the study of the pressure dependences of the resistive characteristics and the shape of superconducting transitions of $Y_{1-x}Pr_xBa_2Cu_3O_{7-\delta}$ compounds (refer for example to [7] and references therein). Furthermore, the results in these studies are often contradictory. For example, it is reported that both the positive and negative baric derivative dT_c/dP were recorded, and in some cases, the sign of dT_c/dP was changed [25].

The approximation of the temperature dependence of the resistivity using the known mechanisms of charge carriers scattering in the normal state and in the transition to the superconducting state makes it possible to obtain a number of parameters characterizing these processes, to relate the parameters to each other, and also to study the influence of external factors on the scattering processes and the transition to the superconducting state. Such well-known mechanisms of charge carriers scattering in the normal state are scattering of carriers by phonons and lattice defects.

In previous work [26, 27], we studied the effect of high hydrostatic pressure up to 17 kbar on the resistive characteristics of poorly doped

praseodymium ($x \approx 0.05$) and excess conductivity ($x \approx 0.23$) single-crystal $Y_{1-x}Pr_xBa_2Cu_3O_{7-\delta}$ samples. Here, we focus on the effect of high hydrostatic pressure up to 11 kbar on the phase separation in the basal ab-plane of medium-doped with Pr ($x \approx 0.23$) single-crystal $Y_{1-x}Pr_xBa_2Cu_3O_{7-\delta}$ samples. We approximate the resistivity temperature dependence in the interval $T_c - 160$ K using the Bloch-Grüneisen relation with the transition to fluctuation conductivity described in accordance with the results of Lorntz-Doniach.

2 Methodology

HTSC single crystals of the $Y_{1-x}Pr_xBa_2Cu_3O_{7-\delta}$ compounds were grown by the solution-melt technology in a gold crucible, according to the procedure reported previously [26]. For resistive studies, rectangular crystals with a size of $3 \times 0.5 \times 0.03$ mm³ were selected. The smallest crystal size corresponds to the c-axis direction. Electrical contacts were created according to a standard 4-contact scheme by applying a silver paste to the crystal surface, followed by connecting silver conductors 0.05 mm in diameter and annealing for three hours at a temperature of 200 °C in an oxygen atmosphere. This procedure made it possible to obtain a contact resistance of less than one Ohm and to carry out resistive measurements at transport currents up to 10 mA in the ab-plane. Hydrostatic pressure was created in a piston-cylinder multiplier [26, 27]. The pressure was determined using a manganin manometer, and the temperature was determined with a copper-constantan thermocouple mounted on the outer surface of the chamber at the level of the sample position.

3 Results and discussion

The pressure dependences (from $p = 0$ to 11 kbar, see also table) of resistivity in the basal plane at room temperature, $\rho_{ab}(300, P)$, and the corresponding derivative, $(d[\ln\rho_{ab}(300, P)])/dP$ of the $Y_{0.77}Pr_{0.23}Ba_2Cu_3O_{7-\delta}$ single crystal are shown in Fig. 1. At atmospheric pressure, $\rho_{ab}(300, 0)$ was ≈ 333 $\mu\text{Ohm}\cdot\text{cm}$. Thus, in comparison with the pure single-crystal $YBa_2Cu_3O_{7-\delta}$ samples, $\rho_{ab}(300, 0)$ increased by ≈ 120 $\mu\text{Ohm}\cdot\text{cm}$, which generally agrees with the literature data. The reasons for the degradation of the

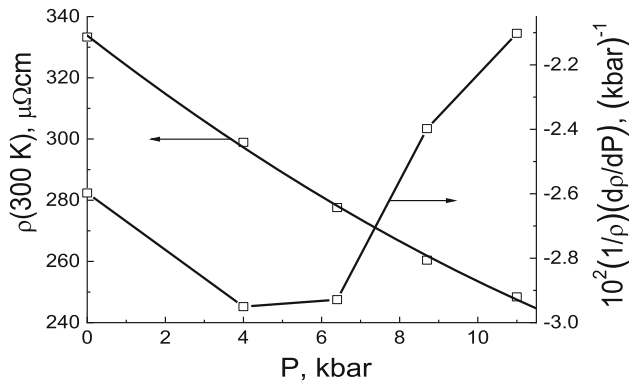


Fig. 1 Dependences $\rho_{ab}(300, P)$ and derivative, $(d[\ln\rho_{ab}(300, P)])/dP$

conducting characteristics of $YBa_2Cu_3O_{7-\delta}$ compounds upon doping with praseodymium (“praseodymium anomaly”) are analyzed in detail previously [7].

$\rho_{ab}(300, P)$ and the derivative, $d[\ln\rho_{ab}(300, P)]/dP$, depend on pressure primarily due to a decrease in volume, that is, due to an increase in the Debye temperature, θ , and, at sufficiently high temperatures, $\rho \propto \theta^{-2}$. Then $d(\ln\rho_{ab})/d(\ln V) = [d(\ln\rho_{ab})/d(\ln\theta)]/[d(\ln\theta)/d(\ln V)] \approx -2\gamma$ [28] and $(1/\rho)(d\rho/dP) = 2\gamma\beta$, where $\beta = -(1/V)(dV/dP)$ and γ – the Grüneisen parameter.

It is observed that the value $(1/\rho)(d\rho/dP) = 2\gamma\beta$ varies within 3–2 $(kbar)^{-1}$, which for $\gamma \approx 2$ gives the value of the volumetric compressibility, $\beta \approx 0.005\text{--}0.007 (kbar)^{-1}$. These values β are in qualitative agreement with previous work [29], where $\beta \approx 0.0085$ was obtained for $YBa_2Cu_3O_x$. The decrease in the compressibility of our sample can be caused both by the presence of Pr and by the inhomogeneity of the sample itself (see Fig. 2).

HTSC is characterized by the presence in the sample of microscopic regions (domains) [30] with different T_c . That is, there is a distribution of T_c over the sample volume. This inhomogeneity of the sample leads to broadening of the superconducting transition to 0.1–1 K in optimally doped HTSCs [31]. Note that the measured effective resistance decreases with decreasing temperature as the single superconducting cluster, consisting of domains that have already transformed into the superconducting state, grows, and in the absence of percolation effects, the decrease in the resistance near the superconducting transition is proportional to the total volume fraction of domains that have already become

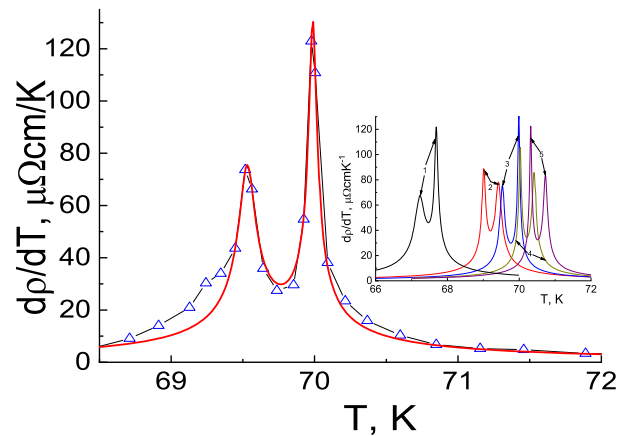


Fig. 2 Derivative, $d\rho_{ab}(T, 6.4 kbar)/dT$, in the superconducting transition region: points—calculated from experimental data $\rho_{ab}(T, 6.4 kbar)$; line—empirical distribution function (1). Box: empirical distribution functions (1) for the pressures used (refer to caption of Fig. 1)

superconducting at a given temperature, $T \leq T_{ci}$. Under such conditions, the only experimentally determined characteristic temperature in the region of the superconducting transition is the temperature of the maximum of the derivative, $d\rho/dT$, and the derivative itself, $d\rho(T \approx T_c)/dT$, is proportional to the distribution function for T_{ci} [32, 33].

Notably, the effective resistance vanishes only when a single cluster is formed from the superconducting domains, extending from one potential contact to another. Since the distribution function for T_{ci} is a consequence of the heterogeneity of a particular sample, it is a characteristic of the sample, and therefore, it should be determined by approximating the function $F(T) = d\rho(T \approx T_c)/dT$ with good empirical relations.

In underdoped samples and samples with defects (impurities, substitutional atoms, etc.), macroscopic regions with their own T_c distributions over the region’s volume can form, leading in turn to a multistep superconducting transition [34]. According to the well-known parabolic dependence [35], each of these phases is characterized by the corresponding concentration of current carriers. In this case, the distribution function for T_{ci} is the sum of the corresponding functions $F_i(T)$.

Figure 2 shows the derivative, $d\rho_{ab}(T)/dT$, in the superconducting transition region for one of the pressures (6.4 kbar) and the corresponding empirical function. This empirical function is the sum

$F(T) = F_l(T) + F_h(T)$, where $F_l(T)$ and $F_h(T)$ have the next form

$$F_i(T) = \frac{b_i}{\sqrt{(T^2 - T_{ci}^2)^2 + (w_i T)^2}} \quad (1)$$

Here $i = h, l$; T_{ci} , b_i , and w_i are parameters determined by the least-squares method. The average approximation error is close to 3%. The values of these parameters are presented in Table 1.

In Fig. 2 the empirical function (1) describes well the derivative, $d\rho_{ab}(T, 6.4 \text{ kbar})/dT$, in the entire region of the superconducting transition, except for the lowest-temperature region $T < 69.5 \text{ K}$, where one more distribution of the type (1), the parameters of which are difficult to determine due to the small number of experimental points.

The insert in Fig. 2 demonstrates the shift of the $d\rho_{ab}(T, P)/dT$ maxima in the superconducting transition region toward higher temperatures when hydrostatic pressure is applied. In this case, the heights of the maxima change in an arbitrary way; that is, with each cooling down, its own distribution of T_c is created, only qualitatively corresponding to the previous one. It can be seen from the table that only T_{ci} increase monotonically with increasing pressure. The parameters b_i and w_i show a non-monotonic behavior versus pressure. An exception is a height of the lower-temperature maximum, $(d\rho/dT)_{lmax}$, which tends to increase with increasing pressure. Such a change in the steepness of the steps indicates a change in the paths of current flow after annealing the crystals at room temperature, which is possible with a change in the spatial distribution and sizes of clusters of the low- and high-temperature phases.

The width of the superconducting transition is determined by the inhomogeneity of the sample—for

example, fluctuations of its composition [36]. These inhomogeneities lead to the appearance in the sample of regions with their own local transition temperature, and the transition in these regions occurs independently of the state of the neighboring regions. As noted above, the homogeneous state of HTSCs with defects is unstable—it is energetically favorable to split HTSCs into domains $l \sim 10^{-5} \text{ cm}$ in size with high and low conductivities (metallic regions with small δ ($\delta < 0.15$) and poorly conducting regions with large δ ($\delta > 0.3$)). For the case of ferroelectric phase transitions, such regions are called Kenzig regions [37], the size of which is also estimated as $l \sim 10^{-5} - 10^{-6} \text{ cm}$, ($a < l < L$, a is the crystal lattice constant, L is the sample size). It can be assumed that the width of a one-step superconducting transition—the width of one maximum $d\rho_c(T)/dT$ at half its height—is determined by just such mesoscopic fluctuations in the concentration of defects—oxygen vacancies or impurity atoms.

The appearance after Pr doping of a two-step superconducting transition (two maxima $d\rho_c(T)/dT$) indicates the appearance of at least two macroscopic regions with different, lower than in the initial state, transition temperatures. Clearly, each of these regions has its own transition width generated by mesoscopic fluctuations in the concentration of defects in this region.

Note that the vanishing of resistance is due to the formation of a single superconducting cluster extending from one potential contact to another and shunting all other, both normal and superconducting regions if any. Thus, doping with Pr led to the appearance, along with mesoscopic, macroscopic inhomogeneities, which caused a two-step superconducting transition, shifted to the region of lower

Table 1 Values of the parameters of the empirical function (1)

		P, kbar	0	4.1	6.4	8.7	11
Low	T_{cl} , K		67.23	69.01	69.53	70.03	70.32
	w_l , K		0.244	0.0861	0.110	0.0615	0.0513
	b_l , $\mu\Omega \cdot \text{cm} \cdot \text{K}$		949	454	524	415	408
	$F(T_{cl})$		67.5	88.8	75.6	105.73	122.57
High	T_{ch} , K		67.69	69.42	69.99	70.41	70.73
	w_h , K		0.0828	0.149	0.0520	0.0985	0.102
	b_h , $\mu\Omega \cdot \text{cm} \cdot \text{K}$		601	726	447	542	550
	$F(T_{ch})$		121.91	78.3	130.3	85.8	83.6

The error of the given data is equal to one in the last digit

temperatures, and the steps of which expand with an increase in the concentration of Pr.

Thus, the spatial distribution of defects created by the Pr impurity leads (along with mesoscopic fluctuations) to the observation of macroscopic fluctuations in the concentration of defects. It is most likely that such macroscopic regions with different defect concentrations are separate phase clusters in the **ab**-planes of the $\text{YBa}_2\text{Cu}_3\text{O}_{7-\delta}$ single crystal.

A similar temperature dependence of the resistance was previously determined [38] for an amorphous Zr-Rh alloy in the range of 4.8–298 K and is attributed by the authors to a possible spatial inhomogeneity of this alloy. Ivanov and Loktev [30], referring to the experimental data on the separation of $\text{La}_2\text{CuO}_{4+\delta}$ into metallic regions with large and dielectric regions with small (the size of the regions is $\sim 10^{-5}$ cm), substantiate the energetic advantage of dividing HTSC into domains with high and low conductivities. Of course, the splitting process is controlled by the diffusion of the corresponding ions, which is relatively low even near room temperatures. Nevertheless, the homogeneous state of HTSC with defects is unstable [30].

The phase separation under pressure observed in the present study can be due to different sizes and compositions of clusters characterized by different contents of Pr [7]. It should be noted that an increase in the Pr content in a local volume element of an experimental sample, as a rule, leads to a diametrically opposite effect of an increase in the oxygen content. While an increase in the oxygen concentration leads to an increase in T_c and an improvement in the conducting characteristics of an individual phase [17], an increase in the Pr content contributes to the suppression of conductivity and a decrease in T_c [7]. A particular role in this can be played by structural and kinematic anisotropy in the system [39–43]. Thus, it can be assumed that the phase separation observed in the compound of the $\text{Y}_{0.77}\text{Pr}_{0.23}\text{Ba}_2\text{Cu}_3\text{O}_{7-\delta}$ single crystal under high pressure, in contrast to the case of pure $\text{YBa}_2\text{Cu}_3\text{O}_{7-\delta}$ samples, is a more complex and ambiguous process. Verifying the validity of this assumption requires additional studies of the effect of uniform compression on the critical temperature of compounds $\text{Y}_{1-x}\text{Pr}_x\text{Ba}_2\text{Cu}_3\text{O}_{7-\delta}$, including a broader range of Pr concentrations, as well as using structural measurements on samples with a higher degree of doping with Pr.

The temperature dependence of the sample resistivity was approximated by the relations

$$\rho_{ab}(T) = (\rho^{-1} + \Delta\sigma_{LD})^{-1}; \rho = (\rho_0 + \rho_3 + \rho_5) \times (1 - b_0 \times T^2) \tag{2}$$

$$\rho_n = C_n \left(\frac{T}{\theta}\right)^n \int_0^{\theta/T} \frac{x^n e^x}{(e^x - 1)^2} dx; \Delta\sigma_{LD} = \left(\frac{e^2}{16\hbar d}\right) \varepsilon^{-1} (1 + J\varepsilon^{-1})^{-1/2} \tag{3}$$

Here ρ_0 is the residual resistivity due to the charge carriers scattering on defects; θ is the Debye temperature; ρ_3, ρ_5 are the resistivities due to scattering of charge carriers by phonons (Bloch-Gruneisen relation), ρ_3 characterizes the interband scattering, and ρ_5 characterizes the intraband scattering [44]; b_0 characterizes the change in the shape of the curve of the density of electronic states by increasing the temperature [45]; $\Delta\sigma_{LD}$ is the Lawrence-Doniach excess conductivity [46], d is the interplanar distance in the $\text{Y}_{0.77}\text{Pr}_{0.23}\text{Ba}_2\text{Cu}_3\text{O}_{7-\delta}$ single crystal, $\varepsilon \approx (T - T_c) / T_c$, $J = (2\xi_c(0)/d)^2$ is the interplanar pairing constant, and ξ_c is the coherence length along the *c* axis. The temperature of the superconducting (SC) transition was determined from the position of the maximum of $d\rho(T)/dT$, in the region of the superconducting transition, since this temperature is the only experimentally determined temperature characterizing the superconducting transition.

The approximation parameters (2)-(3) are given in Table 2. When calculating the values of $\xi_c(0)$, the decrease in the interplanar distance, d , with increasing pressure was calculated according to the data of [29].

Figure 3 shows the $\rho_{ab}(T)$ dependences at various pressures and the corresponding approximating curves for the $\text{Y}_{0.77}\text{Pr}_{0.23}\text{Ba}_2\text{Cu}_3\text{O}_{7-\delta}$ single crystal. It can be seen that the $\rho_{ab}(T)$ dependence does not qualitatively change at all applied pressures and remains metallic. The parameters of the approximation according to Eqs. (2)-(3) are changed—see Table 2.

Inset a shows the SC transition at one of the pressures (11 kbar). The total width of the transition (~ 3 K) and the presence of steps on it indicate the inhomogeneity of the sample, that is, the existence of both macroscopic regions with different T_c and variations in T_c within such macroscopic regions. The kinks of the steps correspond to the maxima of the derivatives

Table 2 The characteristics of superconducting transitions and approximation parameters of the temperature dependence of the resistivity, $\rho_{ab}(T, P)$, according to Eqs. (1)–(2)

P, kbar	0	4.1	6.4	8.7	11
T_c^{high} , K	67.67	69.42	69.98	70.38	70.73
T_c^{low} , K	67.23	69.02	69.52	70.04	70.33
θ , K	279	284	281	279	279
T_c^{high}/θ	0.242	0.244	0.249	0.252	0.254
ρ_0 , $\mu\text{Ohm}\cdot\text{cm}$	58	49	35	34	37
C_3 , $\mu\text{Ohm}\cdot\text{cm}$	71	60	68	65	31
C_5 , $\mu\text{Ohm}\cdot\text{cm}$	1456	1462	1369	1244	1199
b_0 , 10^{-6}K^{-2}	3.1	4.2	5.4	4.8	4.0
J	14.4	7.2	21	18.5	11.4
$\xi_c(0)$, \AA	22	15	26	24	19
Average approximation error, %	1.5	1	1.5	1.5	1.5

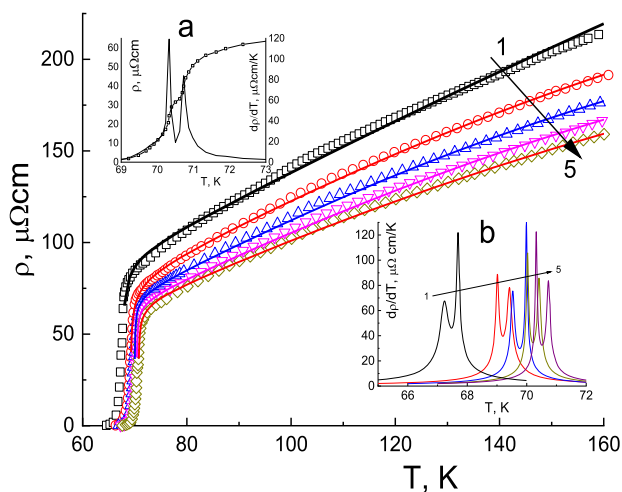


Fig. 3 Temperature dependences of the resistivity in the basal plane of the $\text{Y}_{0.77}\text{Pr}_{0.23}\text{Ba}_2\text{Cu}_3\text{O}_{7.8}$ single crystal at different pressures: 1— $P = 0$; 2—4.1 kbar; 3—6.4 kbar; 4—8.7 kbar; 5—11 kbar. Symbols are the experimental data; lines are the approximations according to (2). Inset a: transition to the superconducting state at $P = 11$ kbar and the corresponding temperature derivative of the resistivity. Inset b: The temperature derivatives of the resistivity in the SC transition region at various pressures

$d\rho/dT$. It can be seen from the Table 1 and inset b that, with increasing pressure, the $d\rho/dT$ maxima shift to higher temperatures, but the distance between the maxima ($\langle T_c^{\text{high}} - T_c^{\text{low}} \rangle \approx 0.4$) does not depend on pressure [47].

The position of the maxima of the derivatives, $d\rho/dT$, and their width depend on the distribution of labile oxygen and Pr within the step. The shift of the maxima (respectively, steps) upon application of pressure indicates the redistribution of, first of all, labile oxygen under the action of pressure. The preservation of the temperature distance between the

maxima indicates that such a redistribution is the same within the entire sample.

The error of the given data is equal to one in the last digit.

Figure 4 shows the temperature dependences of individual terms in (2) in the initial state ($P = 0$). It can be seen that in the normal state, the main contribution to the resistivity comes from the intraband scattering (term ρ_5) and the residual resistance, ρ_0 . The contributions from the interband scattering (term ρ_3) and the corrections due to the change in the shape of the curve of the density of electronic states (factor $1 - b_0 T^2$) are an order of magnitude smaller.

The inset in Fig. 4 shows the conductivity in the Lorentz-Doniach model [46], $\Delta\sigma_{LD}$, in comparison with the total conductivity of the sample in the normal state, $\rho_{ab}(T, P = 0)$. It is seen that at temperatures

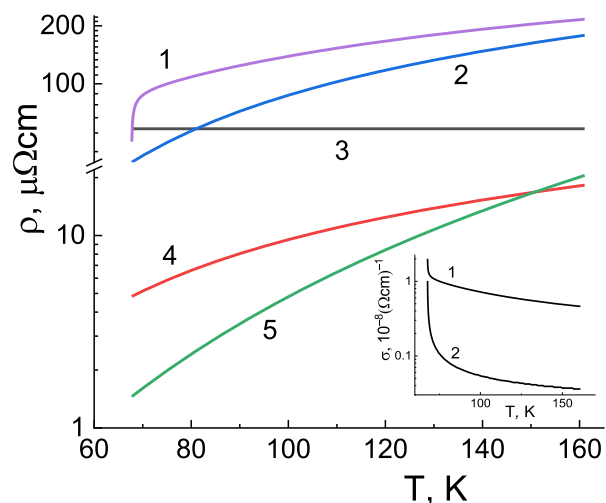


Fig. 4 The values of the terms in (2) for $P = 0$: 1 – total resistivity, $\rho(T)$; 2 – ρ_5 ; 3 – ρ_0 ; 4 – ρ_3 ; 5 – $1 - b_0 T^2$. Inset: 1 – total conductivity, $1/\rho(T)$; 2 – $\Delta\sigma_{LD}$

below a certain one (in this case, at $T \leq 68$ K), the term $\Delta\sigma_{LD}$ prevails.

According to the data [29, 48], at the pressure values we used, the relative decrease in the sample volume does not exceed 1%, while the relative decreases in the approximation parameters (2) are much larger (see Table 2). This means that the increase in the density of conduction electrons under pressure is not the main reason for the decrease in the resistivity of the sample.

In previous work [29], it was noted that the $YBa_2Cu_3O_{7-\delta}$ compounds are characterized by a significant anisotropy of linear compressibility in the directions along and perpendicular to the c axis. This anisotropy of compressibility, which decreases with increasing pressure, was characterized in [29] by the equation $An = [c/3 - (a + b)/2]/V^{1/3}$ (a , b , and c are the unit cell parameters). In Fig. 5, we depicted the relative changes in the approximation parameters according to (2)–(3) depending on pressure, P (lower scale), and anisotropy of linear compressibility, An (upper scale).

In the study of Larkin and Varlamov [49], they described a geometric crossover, when, with decreasing temperature, a transition occurs from the 3D regime $\xi(T) \ll h$ (h is the film thickness) to the 2D regime $\xi(T) \gg h$. Takahashi et al. [50] studied

the decrease in the anisotropy in $Sr_{14-x}Ca_xCu_{24}O_{41+\delta}$ with increasing pressure and associated it with the transition from one-dimensional to two-dimensional conductivity.

The decrease in the anisotropy in $Y_{0.77}Pr_{0.23}Ba_2Cu_3O_{7-\delta}$ with increasing pressure is due to a rapid decrease in the interplanar distance, c , in comparison with parameters a and b . At high pressures, this process can lead to a “baric” crossover from 3 to 2D regime due to a decrease in the interplanar distance (spacing) to $c \leq \xi(T)c$ when pressure is applied.

In Fig. 5, it is seen that under pressure, the greatest relative change is experienced by the parameter b_0 , which, according to Aisaka and Shimizu [45], depends on the shape of the curve of the density of electron states on the Fermi surface; parameters ρ_0 , C_5 , and C_3 show a tendency to decrease with increasing pressure or with decreasing anisotropy; the Debye temperature, θ , obtained from the Bloch–Grüneisen relation does not depend on pressure.

Since $\Delta\theta/\theta \approx \Delta V/V + \Delta F/F$ ($\Delta F/F$ is the magnitude of the interatomic interaction), the constancy of θ (at $\Delta V/V < 0$) means that in the range of used pressures (and the corresponding change in the anisotropy of the linear compressibility) $\Delta F/F \approx -\Delta V/V$ —the enhancement of the interatomic interaction compensates for the decrease in volume.

It was shown by Anshukova et al. [51] that to describe the phonon heat capacity of $RBa_2Cu_3O_x$ samples, three Debye temperatures should be introduced: θ_1 , corresponding to transverse fluctuations, propagating along the c axis, θ_2 , corresponding to transverse fluctuations propagating perpendicular to the c axis, and θ_3 , corresponding to longitudinal fluctuations at that $\theta_3 \sim \theta_2 > \theta_1$. For $YBa_2Cu_3O_x$ $\theta_1 = 90$ K, $\theta_2 = 850$ K and $\theta_3 = 295$ K.

As can be seen from the Table 2, for our sample $\theta \approx 280$ K, that is, charge carriers are scattered mainly by longitudinal fluctuations. Since longitudinal fluctuations are always associated with deformations in all three directions, a decrease in anisotropy with increasing pressure affected them rather weakly, which caused the Debye temperature θ to be constant.

The values of T_c and θ obtained from the experimental dependences $\rho(T)$ would make it possible to determine the electron–phonon interaction constant, λ , from the McMillan relation [52, 53]:

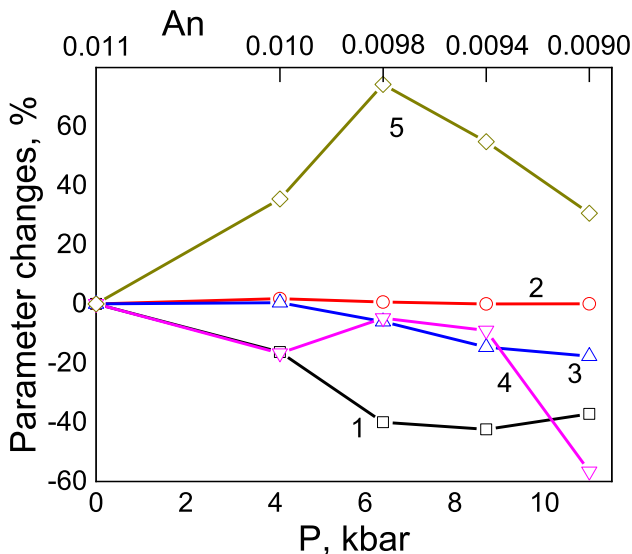


Fig. 5 Relative changes in approximation parameters (2) depending on pressure P (lower scale) or anisotropy of linear compressibility $An = [c/3 - (a + b)/2]/V^{1/3}$ (upper scale). 1 – ρ_0 , 2 – θ , 3 – C_5 , 4 – C_3 , 5 – b_0

$$T_c = \frac{\theta}{1.45} \exp \left[-\frac{1.04(1 + \lambda)}{\lambda - \mu^*(1 + 0.62\lambda)} \right] \quad (4)$$

where μ^* is the effective Coulomb repulsion. However, from (4), it follows that there is a maximum value of the ratio T_c/θ : at $\mu^* = 0$ and $\lambda \rightarrow \infty$ (T_c/θ)_{max} ≈ 0.2438 . For our data, the T_c^{high}/θ ratio increases from 0.242 to 0.254, that is, either it corresponds to unrealistically large values of λ or does not correspond to Eq. (4) at all.

This situation is, in our opinion, due to the fact that the real phonon spectrum of the anisotropic $Y_{0.77}Pr_{0.23}Ba_2Cu_3O_{7-\delta}$ single crystal cannot be described by the Debye model, and the parameter θ , obtained from relations (2)–(3) to the experimental values $\rho_{ab}(T)$ characterizes the type of oscillation on which the charge carriers are scattered. Note that in the study by Fefelov et al. [55], (where the Debye temperature in polycrystalline $YBa_2Cu_3O_x$ was determined from the spin–lattice relaxation time) the value of θ varied from 450 to 280 K for T_c from 74.7 K to 56.3 K, which corresponds to T_c/θ from 0.166 to 0.201. From McMillan's formula, it was found that λ varies from 4 to 10, respectively. It is clear that the adequacy of the McMillan formula is determined in this case by the value of θ , which in an isotropic polycrystal turned out to be greater than in an anisotropic single crystal.

The table also shows that the interplanar pairing constant, $J = (2\xi_c(0)/d)^2$, does not depend on pressure. The calculated (taking into account the dependence $c(P)$ [29]) average value of the coherence length is $\langle \xi_c(0) = (21 \pm 3) \text{ \AA}$. This is an order of magnitude higher than the value obtained by Khadzhai et al. [47]. This discrepancy is probably due to the method of separating excess conductivity. In that study, the excess conductivity was determined by subtracting the low-temperature extrapolation of the high-temperature conductivity from the experimental values, and here, the excess conductivity was determined by subtracting from the experimental values the conductivity, ρ^{-1} , calculated by the formula (eq.) (2)–(3). The large error in the value $\langle J$ is most likely associated with the inhomogeneity of the sample (see inset a in Fig. 3).

The present results are strikingly reminiscent of the following earlier results: In type-II superconductors, high critical current densities can be achieved by the

presence of high-density defects which will provide suitable pinning centers for the magnetic flux lines (e.g., see [55 and references therein]. In such a flux-line pinning, point defects play an important role in $YBa_2Cu_3O_{7-\delta}$ in which doping with alkaline earth elements was found [56] by Su et al. to lead to a formation energy for a Schottky defect which is compatible with the expectations of an early thermodynamical model (e.g., see [57–62]) that interconnects point defect parameters with bulk properties of the material. This model, however, does not seem to describe the case when replacing Y in the doping of $YBa_2Cu_3O_{7-\delta}$ by rare earth elements. The same thermodynamical model was also very recently found by Zhang et al. [63] to show that the activation-free energy gradient controls interfacial mobility in thin polymer films according to molecular dynamics simulations on a layer-by-layer basis.

4 Conclusion

It can be concluded that doping with Pr leads to the appearance of an anisotropic distribution of defects—flat macroscopic superconducting regions with different T_c are formed. Macroscopic superconducting inhomogeneities cause the formation of a multistep superconducting transition, shifted to the region of lower temperatures; the steps of this transition are more extended than in the original transition due to the intensification of mesoscopic inhomogeneities. An increase in the concentration of Pr leads to a decrease in the localization length of charge carriers, which indicates a decrease in the spatial propagation of the wave function of charge carriers. In the normal state, the main contribution to the resistivity of the $Y_{0.77}Pr_{0.23}Ba_2Cu_3O_{7-\delta}$ single crystal is made by intraband scattering ($\propto T^{-5}$) and residual resistivity. Hydrostatic pressure leads to a decrease in the anisotropy of linear compressibility together with a decrease in residual resistivity and phonon resistivity; Debye temperature and coherence length remain constant. The superconducting transition and Debye temperatures obtained from the experimental temperature dependence of the resistivity do not correspond to the McMillan formula, probably due to the large anisotropy.

Authors' contributions

All the authors analyzed and discussed the results and contributed to the writing of the paper.

Funding

No related funding.

Data availability

All data generated or analyzed during this study are included in this published article.

Declarations

Conflict of interest There is no conflict of interest.

Open Access This article is licensed under a Creative Commons Attribution 4.0 International License, which permits use, sharing, adaptation, distribution and reproduction in any medium or format, as long as you give appropriate credit to the original author(s) and the source, provide a link to the Creative Commons licence, and indicate if changes were made. The images or other third party material in this article are included in the article's Creative Commons licence, unless indicated otherwise in a credit line to the material. If material is not included in the article's Creative Commons licence and your intended use is not permitted by statutory regulation or exceeds the permitted use, you will need to obtain permission directly from the copyright holder. To view a copy of this licence, visit <http://creativecommons.org/licenses/by/4.0/>.

References

- R.V. Vovk, A.L. Solovjov, *Low Temp. Phys.* **44**, 81 (2018)
- L. Mendonca Ferreira, P. Pureur, H. A. Borges, P. Lejay, *Phys. Rev. B* **69**, 212505 (2004).
- J.G. Bednorz, K.A. Müller, *Z. Physik B* **64**, 189 (1986)
- Yu.I. Boyko, V.V. Bogdanov, R.V. Vovk, B.V. Grinyov, *Funct. Mater.* **27**, 703 (2020)
- Yu.I. Boyko, V.V. Bogdanov, R.V. Vovk, B.V. Grinyov, *Funct. Mater.* **28**, 415 (2021)
- J. Ashkenazi, *J. Supercond. Nov. Magn.* **24**, 1281 (2011)
- M. Akhavan, *Physica B* **321**, 265 (2002)
- R.V. Vovk, M.A. Obolenskii, A.A. Zavgorodniy, D.A. Lotnyk, K.A. Kotvitskaya, *Physica B* **404**, 3516 (2009)
- M.K. Wu, J.R. Ashburn, C.J. Torng, P.H. Hor, R.L. Meng, L. Gao, Z.J. Huang, Y.Q. Wang, C.W. Chu, *Phys. Rev. Lett.* **58**, 908 (1987)
- A.V. Bondarenko, V.A. Shklovskij, R.V. Vovk, M.A. Obolenskii, A.A. Prodan, *Low Temp. Phys.* **23**, 962 (1997)
- R.V. Vovk, G.Y. Khadzhai, O.V. Dobrovolskiy, *Appl. Phys. A* **117**, 997 (2014)
- R.V. Vovk, Z.F. Nazyrov, L.I. Goulatis, A. Chroneos, *J. Low Temp. Phys.* **170**, 216–222 (2013)
- G.Y. Khadzhai, N.R. Vovk, R.V. Vovk, *Low Temp. Phys.* **40**, 488 (2014)
- R.V. Vovk, N.R. Vovk, G.Y. Khadzhai, I.L. Goulatis, A. Chroneos, *Solid State Commun.* **190**, 18 (2014)
- R.V. Vovk, N.R. Vovk, G.Y. Khadzhai, O.V. Dobrovolskiy, Z.F. Nazyrov, *Curr. Appl. Phys.* **14**, 1779 (2014)
- R.V. Vovk, N.R. Vovk, A.V. Samoilov, I.L. Goulatis, A. Chroneos, *Solid State Commun.* **170**, 6 (2013)
- A.L. Solovjov, E.V. Petrenko, L.V. Omelchenko, R.V. Vovk, I.L. Goulatis, A. Chroneos, *Sci. Rep.* **9**, 9274 (2019)
- D.A. Lotnyk, R.V. Vovk, M.A. Obolenskii, A.A. Zavgorodniy, J. Kováč, M. Kaňuchová, M. Šefciková, V. Antal, P. Diko, A. Feher, A. Chroneos, *J. Low Temp. Phys.* **161**, 387 (2010)
- D.D. Balla, A.V. Bondarenko, R.V. Vovk, M.A. Obolenskii, A.A. Prodan, *Low Temp. Phys.* **23**, 777 (1997)
- A.L. Solovjov, L.V. Omelchenko, E.V. Petrenko, R.V. Vovk, V.V. Khotkevych, A. Chroneos, *Sci. Rep.* **9**, 20424 (2019)
- R.P. Gupta, M. Gupta, *Phys. Rev. B* **51**, 11760–11766 (1995)
- R.V. Vovk, N.R. Vovk, G.Y. Khadzhai, I.L. Goulatis, A. Chroneos, *Physica B* **422**, 33 (2013)
- S. Sadewasser, J.S. Schilling, A.P. Paulicas, B.M. Veal, *Phys. Rev. B* **61**, 741 (2000)
- R.V. Vovk, G.Y. Khadzhai, Z.F. Nazyrov, I.L. Goulatis, A. Chroneos, *Physica B* **407**, 4470 (2012)
- W.-H. Li, S.Y. Wu, Y.-C. Lin, K.C. Lee, J.W. Lynn, S.S. Weng, I.P. Hong, J.-Y. Lin, H.D. Yang, *Phys. Rev. B* **60**, 4212 (1999)
- R.V. Vovk, N.R. Vovk, G.Y. Khadzhai, O.V. Dobrovolskiy, *Solid State Commun.* **204**, 64 (2015)
- G.Y. Khadzhai, A. Chroneos, I.L. Goulatis, S.N. Kamchatnaya, A.L. Chikina, N.R. Vovk, R.V. Vovk, *J. Low Temp. Phys.* **203**, 430 (2021)
- J.M. Ziman. *Electrons and Phonons*. Oxford at the Clarendon Press. 1960, 488 p.
- I.V. Alexandrov, A.F. Goncharov, S.M. Stishov, *JETP Lett.* **47**, 428 (1988)
- M.A. Ivanov, V.M. Loktev, *Low Temp. Phys.* **25**, 996 (1999)

31. G.Y. Khadzhai, C.R. Vovk, R.V. Vovk, *Low Temp. Phys.* **43**, 1119 (2017)
32. S. Kirkpatrick, *Rev. Mod. Phys.* **45**, 574 (1973)
33. J. Maza, F. Vidal, *Phys. Rev. B* **43**, 10560 (1991)
34. H.A. Borges, M.A. Continentino, *Solid State Commun.* **80**, 197 (1991)
35. G. Lacayc, R. Hermann, G. Kaestener, *Physica C* **192**, 207 (1992)
36. B.N. Rolov, V.Je. Jurkevich. Fizika razmytyh fazovyh perehodov. In Russian / B.N. Rolov, V.E. Jurkiewicz. Physics blurred phase transitions. In Russian, 1983. House Rostov University, 1983. 319 p.
37. W. Känzig, *Ferroelectrics and Antiferroelectrics* (Academic Press, New York, 1957), p. 197
38. A.F. Prekul, V.A. Rassokhin, S.V. Yartsev, *JETP Lett.* **38**, 408 (1983)
39. R.V. Vovk, C.D.H. Williams, A.F.G. Wyatt, *Phys. Rev. B* **69**, 144524 (2004)
40. A.J. Matthews, K.V. Kavokin, A. Usher, M.E. Portnoi, M. Zhu, J.D. Gething, M. Elliot, W.G. Herrenden-Harker, K. Phillips, D.A. Ritchie, M.B. Simmons, C.B. Sorensen, O.P. Hansen, O.A. Mironov, M. Myronov, D.R. Leadley, M. Henini, *Phys. Rev. B* **70**, 075317 (2004)
41. D.H.S. Smith, R.V. Vovk, C.D.H. Williams, A.F.G. Wyatt, *Phys. Rev. B* **72**, 054506 (2005)
42. P.G. Curran, V.V. Khotkevych, S.J. Bending, A.S. Gibbs, S.L. Lee, A.P. Mackenzie, *Phys. Rev. B* **84**, 104507 (2011)
43. N. Kuganathan, P. Iyngaran, R. Vovk, A. Chroneos, *Sci. Rep.* **9**, 4394 (2019)
44. L. Colquit, *J. Appl. Phys.* **36**, 2454 (1965)
45. T. Aisaka, M. Shimizu, *J. Phys. Soc. Japan* **28**, 646 (1970)
46. W.E. Lawrence, S. Doniach, *Proceedings of the Twelfth International Conference on Low Temperature Physics*, edited by E.Kanda, Academic Press of Japan, Kyoto, p.361 (1971).
47. G.Y. Khadzhai, N.R. Vovk, R.V. Vovk, *Fiz. Nizk. Temp.* **47**, 388 (2021)
48. V.P. Glazkov, I.N. Goncharenko, V.A. Somenkov. *Solid State Phys.* **30**, (1988).
49. A. Larkin, A. Varlamov. *Theory of Fluctuations in Superconductors*. OUP Oxford, 2005, 432 p.
50. H. Takahashi, N. Mori, T. Nakanishi, T. Nagata, M. Uehara, J. Akimitsu, K. Kinoshita, N. Motoyama, H. Eisaki, S. Uchida, *Rev. High Pressure Sci. Technol.* **7**, 388 (1998)
51. N.V. Anshukova, Yu.V. Bugoslavskii, V.G. Veselago, A.I. Golovashkin, O.V. Ershov, I.A. Zaitsev, O.M. Ivanenko, A.A. Kordyuk, A.A. Minakov, K.V. Mitsen, *JETP Lett.* **48**, 152 (1988)
52. R.C. Dynes, *Solid State Commun.* **10**, 615 (1972)
53. P.B. Allen, R.C. Dynes, *Phys. Rev. B* **12**, 905 (1975)
54. L.K. Aminov, V.A. Ivanshin, I.N. Kurkin, M.R. Gafurov, I.Kh. Salikhov, H. Keller, M. Gutmann, *Physica C* **349**, 30 (2001)
55. O.V. Fefelov, J. Bergli, Y.M. Galperin, *Phys. Rev. B* **75**, 172107 (2007)
56. H. Su, D.O. Welch, W. Wong-Ng, *Phys. Rev.* **70**, 054517 (2004)
57. K. Alexopoulos, P. Varotsos, *Phys. Rev. B* **24**, 3606–3609 (1981)
58. P. Varotsos, K. Alexopoulos, *Phys. Rev. B* **22**, 3130 (1980)
59. P. Varotsos, K. Alexopoulos. *Phys. Rev. B* **24**, 904 (1981)
60. A. Chroneos, R.V. Vovk, *Solid State Ionics* **274**, 1–3 (2015)
61. M.W.D. Cooper, R.W. Grimes, M.E. Fitzpatrick, A. Chroneos, *Solid State Ionics* **282**, 26–30 (2015)
62. A. Chroneos, *Appl. Phys. Rev.* **3**, 041304 (2016)
63. W. Zhang, F.W. Starr, J.F. Douglas, *Chem. Phys.* **155**, 174901 (2021)

Publisher's Note Springer Nature remains neutral with regard to jurisdictional claims in published maps and institutional affiliations.